

EXPERIMENTAL MODELING OF BORA WIND LOADS ON ROAD VEHICLES

Hrvoje Kozmar, Ahsan Kareem

Summary

The Bora is a very strong and gusty downslope wind that blows from the northeast across the coastal mountain ranges on the eastern coast of the Adriatic Sea. It creates substantial difficulties for engineering infrastructure, traffic, and life in general. While the effects of the quasi-steady turbulent atmospheric boundary layer flow on road vehicles are currently fairly well known, the Bora wind also creates unsteady aerodynamic loads on these vehicles, which are still not fully understood. These gust effects on road vehicles have thus been experimentally examined here. This study was conducted on a small-scale road vehicle model, which to our knowledge is the first study of this type. Particular emphasis was placed on the aerodynamic forces and moments experienced by the road vehicle related to the strength and frequency of the Bora wind gusts, the vertical wind incidence angle, and the vehicle position on the bridge. In the experiments regarding the wind gust strength and frequency, the road vehicle model was placed in the upwind traffic lane at zero horizontal and vertical flow incidence angles. The effect of the vertical wind incidence angle and vehicle position was analyzed for the road vehicle model placed in the upwind, middle, and downwind traffic lanes of the bridge-deck section model, where the horizontal flow incidence angle was zero, while the vertical flow incidence angle was studied from 0° to 50° . The experiments were carried out in the Transient Flow Field Simulator of the Nat-Haz Modeling Laboratory at the University of Notre Dame, USA. The results reveal some important findings. Regarding the wind gust strength and frequency experiments, the aerodynamic loads rose linearly with increasing gust strength and were concurrently affected by vortex shedding and wind gusting phenomena. The steady aerodynamic loads were generally higher for a road vehicle closer to the upwind edge of the bridge decks. The wind gusting of the Bora can cause difficulties for the maneuvering of road vehicles and for their stability in the upwind traffic lane, while the risk for road vehicles in the downwind traffic lanes was predominantly a

consequence of the impinging shed vortices unique to bridge architecture and the aerodynamic form of vehicles.

Keywords: gusty Bora wind, aerodynamic loads on road vehicles, laboratory experiments.

1. INTRODUCTION

The Bora is a very strong, usually dry and always gusty wind that blows from the northeast across the coastal mountain ranges on the eastern coast of the Adriatic Sea, e.g. Yoshino (1976), Bajić (1988, 1989), Tutiš (1988), Vučetić (1991), Belušić and Klaić (2004, 2006). It more commonly occurs in winter when it can last from several hours up to several days, e.g. Jurčec (1981), Poje (1992), Enger and Grisogono (1998), Jeromel et al. (2009). Its mean velocity, usually not less than 5 m/s and often surpassing 30 m/s, is less significant than its gusts that can reach velocities up to five times the average, e.g. Petkovšek (1987), Grisogono and Belušić (2009), Večenaj et al. (2010), Belušić et al. (2013). There is no precise definition of the Bora, primarily due to its extreme spatial variability, e.g. Horvath et al. (2009), Večenaj et al. (2012). However, its basic characteristics are that it is a horizontal wind with an azimuth from the first quadrant lasting at least for three hours with a mean wind speed higher than 5 m/s and a standard deviation comparable to the mean value.

Bora wind gusts are a consequence of cold air cylinders rolling down the slope on the warm side of a mountain ridge. Along with the atmospheric turbulence and sliding cold air, the concurrent action of these three phenomena creates a complex wind flow and turbulence with characteristic Bora features, Figure 1.

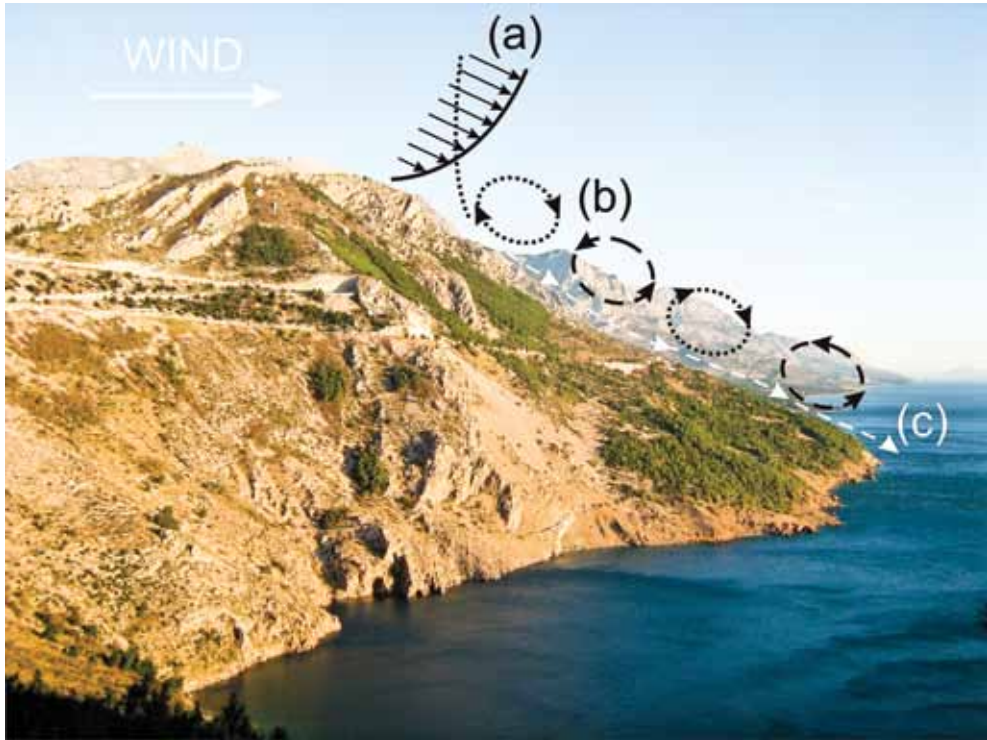


Figure 1. Elements of the gusty Bora wind: a) atmospheric wind flow and turbulence (the solid line is the mean velocity profile and the dotted line is the turbulence kinetic energy profile); b) air cylinders exerted by orographic wave breaking; c) sliding cold air. Photograph taken by Tomica Kozmar in the Dubci area, 40 km south of Split, Croatia, after Kozmar et al. (2012a)

Slika 1. Elementi mahovitog vjetra bure: a) atmosferski vjetar i turbulencija (puna crta je profil osrednjene vrijednosti brzine, isprekidana crta je profil kinetičke energije turbulencije), b) vrtlozi zraka nastali lomljenjem orografskog vala, c) klizajući hladan zrak. Fotografiju snimio Tomica Kozmar na području Dubaca, 40 km južno od Splita, Hrvatska, Kozmar i sur. (2012a)

The characteristics of the Bora wind have been previously analyzed in meteorology, climatology, and geophysics. However, the focus of these works was quite different from what is required for input information for environmental and structural aerodynamics. In other words, the existing data are of rather marginal relevance for engineering applications. This was therefore motivation for the joint work of geophysicists and engineers to address the Bora and other non-synoptic winds in a form suitable for engineering applications, e.g. Lepri et al. (2014, 2015, 2017), a special issue of *Wind and Structures* (Kozmar, 2017), Hangan and Kareem (2021).

There is a substantial body of knowledge on aerodynamic loads acting on road vehicles subjected to quasi-steady turbulent cross flows. In these quasi-steady conditions, three types of wind-induced vehicle accidents are possible, i.e. overturning, side-slip, and rotation. Baker (1986, 1987, 1991a,b,c) extensively studied the performance of high-sided vehicles in cross winds and proposed equations to account for the wind effects on vehicles. For high-sided vehicles like buses and trucks, overturning is more likely to occur than the other two types of accidents. A gust duration of only 2 s to 3 s was seen to be sufficient to blow over a vehicle, Baker and Robinson (1990). The wind speed at which the accident criteria are exceeded is a function of vehicle speed, wind direction, and the infrastructure. Meteorological data may be used to determine the time period, the accident wind speed, and the risk probability, Baker and Reynolds (1992). This brief survey reveals that quasi-steady cross winds may create a substantial risk for vehicles, while this issue is even more complex for transient winds like the Bora.

Preliminary studies on the effects of transient wind loads on vehicles have shown that the steady-state approach underestimates transient forces and moments, Ryan and Dominy (1998), while the aerodynamic forces exerted only by wind gusts may possibly be predicted by assuming the quasi-steady flow, Bearman and Mullarkey (1994). Currently, there is clearly a substantial lack of knowledge on this topic, a fact which provided motivation for the present work.

Laboratory experiments on the effects of the gusty Bora wind on road vehicles are reported here. Specifically, the aerodynamic loads on road vehicles on bridges were the subject of analysis because vehicles in this configuration are particularly sensitive to cross-wind loading. The aerodynamic forces and moments experienced by road vehicles were studied relating to the strength and frequency of the wind gusts of the Bora, the vertical wind incidence angle, and the vehicle position on the bridge. The study presents an overview of the experimental analysis performed so far and published as journal articles and conference contributions, Kozmar et al. (2009, 2011, 2012a,b, 2015). The contents of these previous publications were adopted or adapted for the purposes of the present study. However, respective references are not provided on each and every occasion in the present article to enhance readability by avoiding disruptions that could occur with excessive referencing.

2. METHODOLOGY

Experiments were carried out in the Transient Flow Field Simulator (TFFS) in the NatHaz Modeling Laboratory at the University of Notre Dame, USA. The TFFS test section equipped with four fans creating the airflows is presented in Figure 2.

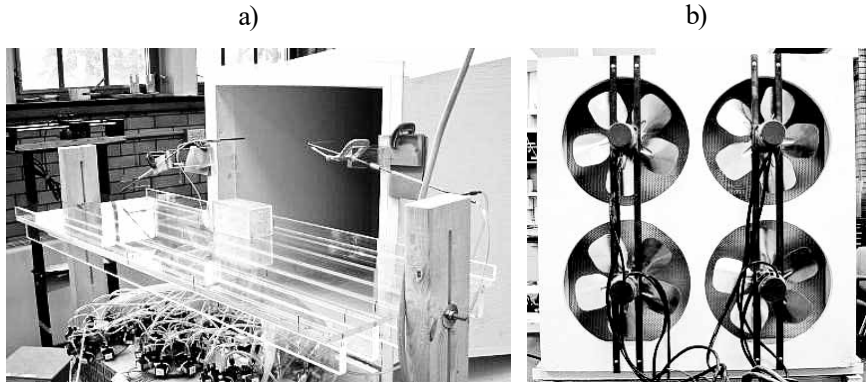


Figure 2. Transient Flow Field Simulator (TFFS) in the NatHaz Modeling Laboratory at the University of Notre Dame, USA. a) test section with a vehicle model on a bridge-deck section model; b) four fans creating the airflows, Kozmar et al. (2012a)

Slika 2. Simulator polja nestacionarnog strujanja zraka (TFFS) u sklopu NatHaz laboratorija Sveučilišta Notre Dame u SAD-u. a) ispitna sekcija s modelom vozila na modelu sekcije mosta, b) četiri ventilatora koji stvaraju strujanje zraka, Kozmar i sur. (2012a)

The TFFS is an open-circuit type wind tunnel with a 50 cm wide and 50 cm high rectangular open test section and a set of four fans that create transient flows. Its general purpose is to allow study of the effect of gusty winds on structural models. Upstream of the structural model, the air flows through a honeycomb, two sets of screens and a nozzle with a contraction ratio of 2:1. At the inlet of the test section, a maximal velocity of ~ 5 m/s can be achieved. The fans are connected to low-inertia BLM-N23-1000 brushless AC servomotors with a 1000 line differential quadrature encoder. The motors are controlled by a Galil DMC-2143 Ethernet system programmed using Labview and Matlab.

Instantaneous velocities in the x -direction were measured using a constant temperature hot-wire probe (DANTEC 54T30) and an eight-channel MINICTA anemometer system. x , y , and z are the main flow, lateral and vertical directions of the Cartesian coordinate system, respectively. The velocity signals were sampled using a 12-bit digitizer

Another set of experiments was carried out to investigate the effect of the vertical wind incidence angle and vehicle position on the bridge on the aerodynamic loads experienced by Bora wind gusting. In these experiments, the vehicle model was placed in the center of the upwind, middle, and downwind traffic lanes, Figure 4.

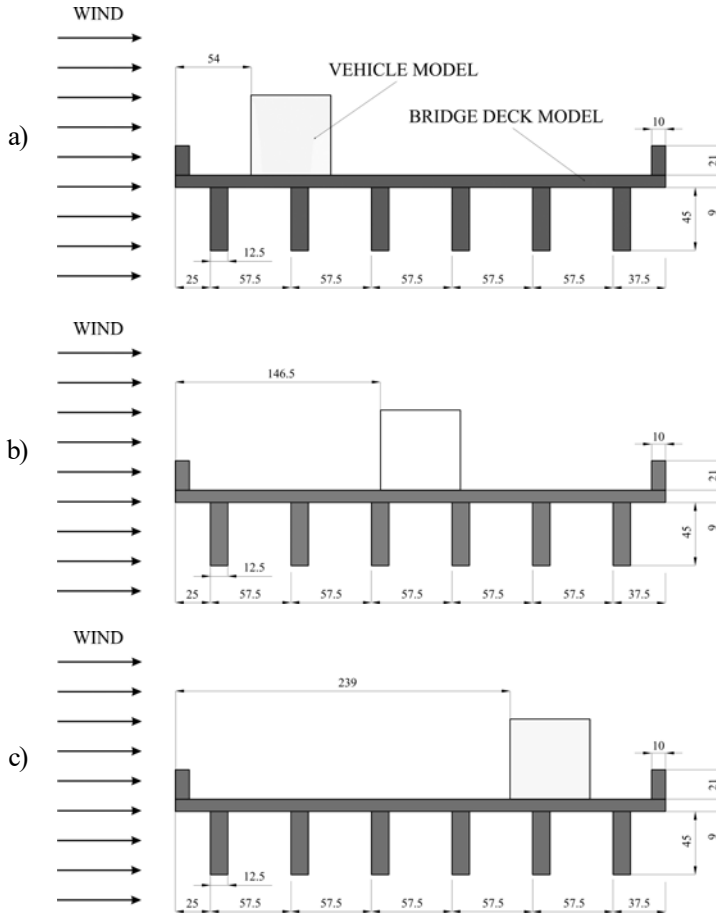


Figure 4. Experimental setup for the vehicle model on the bridge-deck section model: a) vehicle model in the upwind traffic lane; b) vehicle model in the middle traffic lane; c) vehicle model in the downwind traffic lane; all dimensions are provided in mm on the model scale, Kozmar et al. (2015)

Slika 4. Eksperimentalni postav modela vozila na modelu sekcije mosta: a) model vozila u prometnoj traci uz vjetar, b) model vozila u srednjoj prometnoj traci, c) model vozila u prometnoj traci niz vjetar; sve dimenzije su dane u mm na skali modela, Kozmar i sur. (2015)

The pedestrian pathway along the bridge is taken to be 1.45 m and a single traffic lane 3.7 m wide that gives a distance between the leading edge of the bridge deck and the vehicle center of 3.3 m, all in full-scale dimensions, i.e. 3.3 m is 82.5 mm on the model-scale calculated using the simulation length scale of 1:40. The 1.8 m full-scale height of the I-beams was selected, which is a common design of freeway bridges. All model parts were manufactured of Plexiglas on a 1:40 simulation length scale. The bridge-deck section model was placed 50 mm downstream of the nozzle exit and rigidly fixed to avoid flow disturbances.

Longitudinal turbulence intensity I_u at the position of the vehicle model (center of the cross section) was 8%, both during the gusts and 'regular' (weak) wind periods, and the maximal mean flow velocity was $\bar{u} = 4.5$ m/s. Reynolds number (Re) effects were observed for $Re < 14000$. For $Re > 14000$, possible errors in the side force coefficient C_{FS} and the lift force coefficient C_{FL} are 16% and 3%, respectively, which is acceptable for the present study where the fundamental flow and loading phenomena were to be clarified. All subsequent experiments were accordingly conducted at $Re > 14000$.

The side force F_s and overturning (rolling) moment M_R of the vehicle were studied because they are generally considered important parameters when investigating the cross-wind loading of vehicles. The effects of Bora wind gusts were simulated by exposing the vehicle model to an airflow which consisted of intermittent switching between weak wind (smaller velocity) and wind gusts (larger velocity).

The horizontal flow incidence angle on the bridge-deck section and vehicle model was 0° in all experiments. The vertical flow incidence angle α was 0° in the experiments regarding the wind gust strength and frequency, while in the experiments regarding the effects of α and the vehicle position on the bridge deck, it was in the range of $0^\circ < \alpha < 50^\circ$, Figure 5.

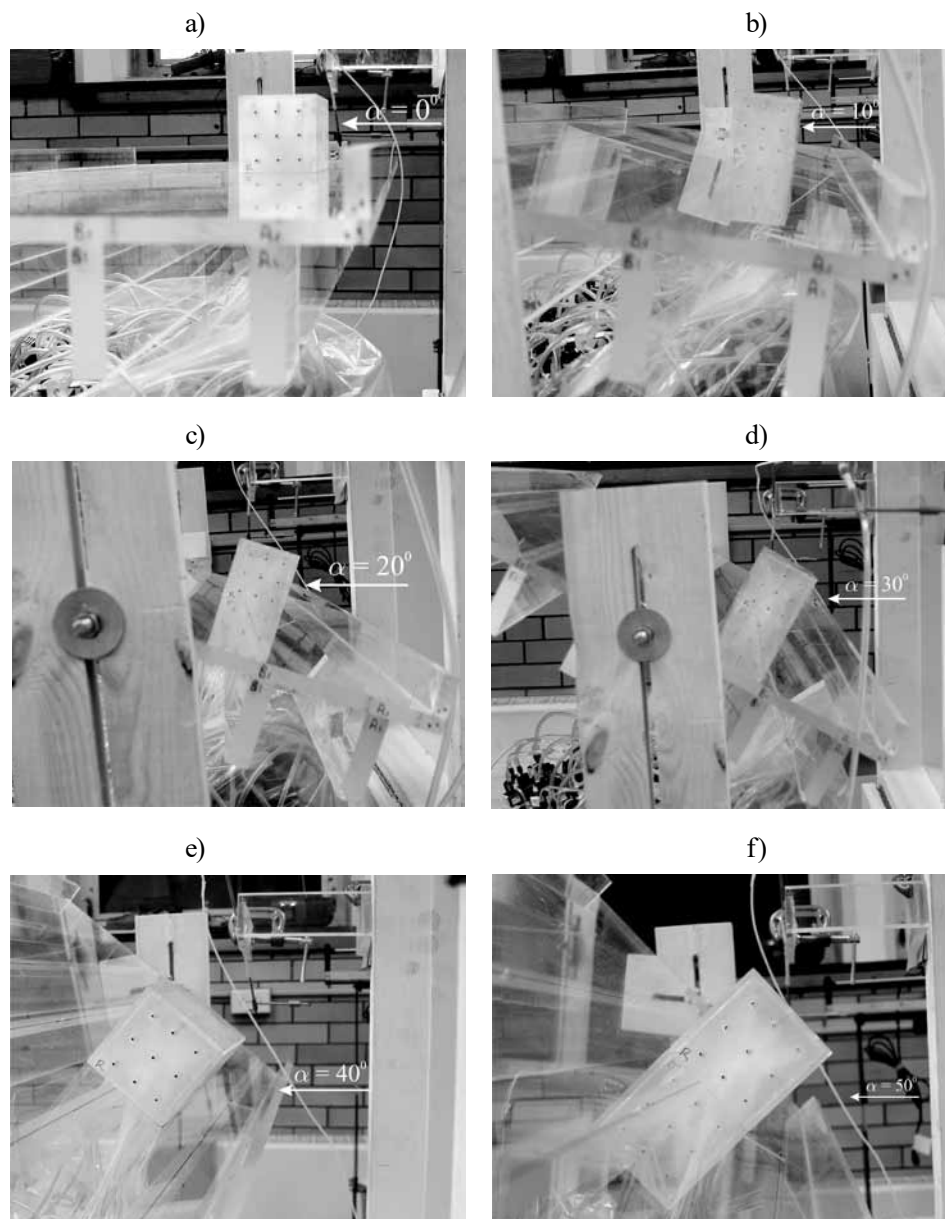


Figure 5. Vehicle model on the bridge-deck section model at various vertical flow incidence angles, Kozmar et al. (2015)

Slika 5. Model vozila na modelu sekcije mosta pri različitim vertikalnim kutovima nstrujavanja zraka, Kozmar i sur. (2015)

By varying α , the experiments aimed to simulate the Bora wind loading of vehicles in the vicinity of hills of various slope angles.

3. RESULTS

The effect of Bora wind gust strength and frequency on the aerodynamic loading of a vehicle was studied first. The gust strength ratio was determined given the maximal possible flow velocity in the TFFS, and minimal flow velocity regarding the Re sensitivity. While it is possible in the TFFS facility to obtain a ratio of flow gust to ‘regular’ wind velocity equal to 1.3, in Bora wind events in nature this ratio can be as high as five, so the effect of even stronger wind gusts on vehicles remains to be studied in the future. The time history and details of five different flow velocity records (for the u flow velocity component in the main flow direction) characterized by the gust duration $\Delta t_G = 4$ s and the duration of ‘regular’ wind events $\Delta t_R = 4$ s are given in Figure 6 and Table 1. \bar{u}_G is the mean flow velocity in the x -direction during gusts, \bar{u}_R is the mean flow velocity in the x -direction during ‘regular’ (weak wind) periods, t is the time, Δt_G is the time duration of gusts, and Δt_R is the time duration of ‘regular’ wind events.

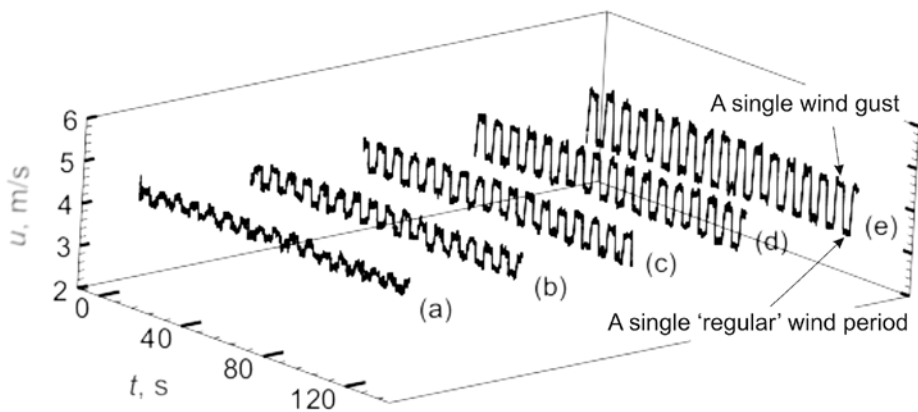


Figure 6. Velocity records for five gust strengths characterized by $\Delta t_R = 4$ s and $\Delta t_G = 4$ s, Kozmar et al. (2012a)

Slika 6. Zapisi brzine za pet jakosti udara bure karakteriziranih s $\Delta t_R = 4$ s i $\Delta t_G = 4$ s, Kozmar i sur. (2012a)

Table 1. Details of velocity time records shown in Figure 6 characterized by $\Delta t_R = 4$ s and $\Delta t_G = 4$ s, Kozmar et al. (2012a)

Tablica 1. Pojediniosti vremenskih zapisa brzine prikazanih na slici 6, karakteriziranih s $\Delta t_R = 4$ s i $\Delta t_G = 4$ s, Kozmar i sur. (2012a)

	(a)	(b)	(c)	(d)	(e)
\bar{u}_R , m/s	4.24	4.03	3.85	3.65	3.44
\bar{u}_G , m/s	4.45	4.45	4.45	4.45	4.46
\bar{u}_G/\bar{u}_R	1.05	1.10	1.16	1.22	1.30

The experiments were also conducted for $\Delta t_R = 3$ s and $\Delta t_G = 2$ s, and for $\Delta t_R = 2$ s and $\Delta t_G = 3$ s, Tables 2 and 3, respectively.

Table 2. Details of velocity time records characterized by $\Delta t_R = 3$ s and $\Delta t_G = 2$ s, Kozmar et al. (2012a)

Tablica 2. Pojediniosti vremenskih zapisa brzine karakteriziranih s $\Delta t_R = 3$ s i $\Delta t_G = 2$ s, Kozmar i sur. (2012a)

	(f)	(g)	(h)	(i)	(j)
\bar{u}_R , m/s	4.42	4.19	3.92	3.71	3.44
\bar{u}_G , m/s	4.62	4.64	4.58	4.59	4.56
\bar{u}_G/\bar{u}_R	1.05	1.11	1.17	1.24	1.33

Table 3. Details of velocity time records characterized by $\Delta t_R = 2$ s and $\Delta t_G = 3$ s, Kozmar et al. (2012a)**Tablica 3.** Pojediniosti vremenskih zapisa brzine karakteriziranih s $\Delta t_R = 2$ s i $\Delta t_G = 3$ s, Kozmar i sur. (2012a)

	(k)	(l)	(m)	(n)	(o)
\bar{u}_R , m/s	4.34	4.12	3.91	3.67	3.41
\bar{u}_G , m/s	4.55	4.55	4.57	4.56	4.52
\bar{u}_G/\bar{u}_R	1.05	1.10	1.17	1.24	1.33

Each experiment consisted of twenty ‘gust’ events and twenty ‘regular’ wind events. The side force and overturning (rolling) moment coefficients, i.e. C_{FS} and C_{MR} , respectively, were normalized using \bar{u}_R . The sign convention was based on Coleman and Baker (1994). The spatial scale L is related to the time scale T using the $L = U \cdot T$ relation, where U is the flow velocity scale. The timescales are the spatial scales divided by appropriate flow velocity. The mean ‘regular’ wind velocity in nature can be taken as 16 m/s. In the TFFS, the mean ‘regular’ wind velocity was approximately 4 m/s and the simulation length scale was 1:40. The time scale 1:10 was thus accordingly adopted.

Figures 7-9 show the dimensionless power spectral density of the longitudinal flow velocity fluctuations $f \cdot S_u(f) / \sigma_u^2$ for the time records reported in Tables 1-3, respectively. f is the frequency, $S_u(f)$ is the power spectral density, and σ_u^2 is the variance.

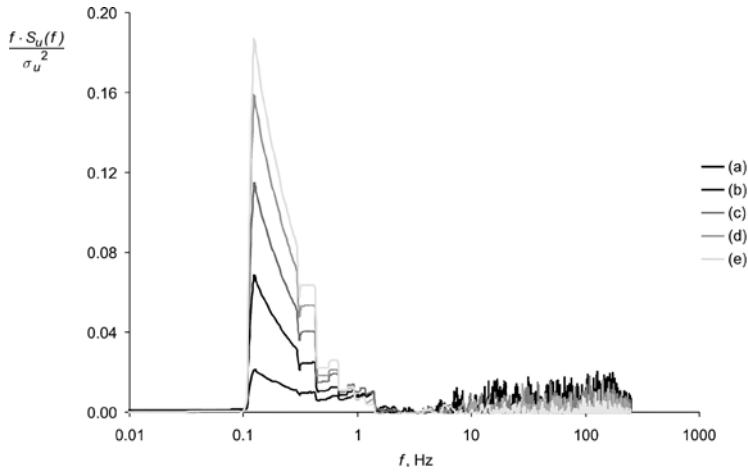


Figure 7. Power spectral density of the longitudinal velocity fluctuations of the flow velocity records presented in Table 1 ($\Delta t_R = 4$ s and $\Delta t_C = 4$ s), Kozmar et al. (2012a)

Slika 7. Spektralna gustoća snage uzdužnih pulzacija brzine strujanja zraka za eksperimente navedene u Tablici 1 ($\Delta t_R = 4$ s and $\Delta t_C = 4$ s), Kozmar i sur. (2012a)

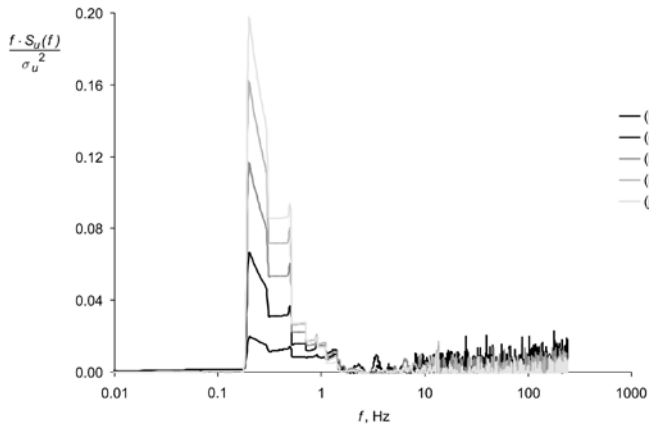


Figure 8. Power spectral density of the longitudinal velocity fluctuations of the flow velocity records presented in Table 2 ($\Delta t_R = 3$ s and $\Delta t_C = 2$ s), Kozmar et al. (2012a)

Slika 8. Spektralna gustoća snage uzdužnih pulzacija brzine strujanja zraka za eksperimente navedene u Tablici 2 ($\Delta t_R = 3$ s and $\Delta t_C = 2$ s), Kozmar i sur. (2012a)

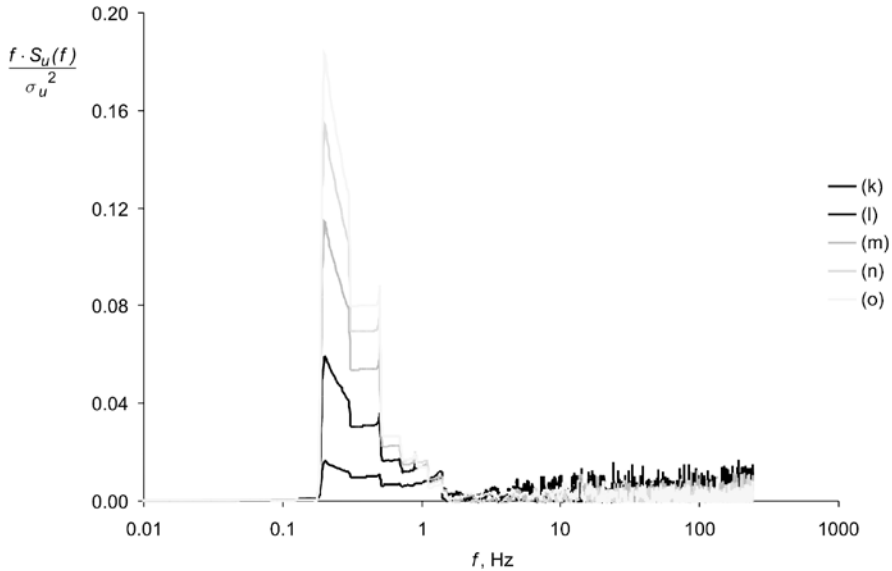


Figure 9. Power spectral density of the longitudinal velocity fluctuations of the time series presented in Table 3 ($\Delta t_r = 2$ s and $\Delta t_G = 3$ s), Kozmar et al. (2012a)

Slika 9. Spektralna gustoća snage uzdužnih pulzacija brzine strujanja zraka za eksperimente navedene u Tablici 3 ($\Delta t_r = 2$ s and $\Delta t_G = 3$ s), Kozmar i sur. (2012a)

The spectral peak can be observed at 0.125 Hz for the (a) to (e) records, and at 0.2 Hz for (f) to (o), which is the effect of intermittent switching between lower and higher flow velocity. These spectral peaks correspond to wind gusts from 50 s to 80 s duration in nature. Another important feature is the energy distribution during wind gusts as the energy of the spectral peaks increases when the wind gusting becomes stronger, i.e. at higher \bar{u}_G / \bar{u}_R ratios. This trend was observed for all repetition rates of the wind gusting.

These flow features have important implications for the steady aerodynamic loading of vehicles, Figures 10 and 11. C_{FS}^{gust} is the mean side force during gusts and $C_{FS}^{regular}$ is the mean side force in ‘regular’ wind.

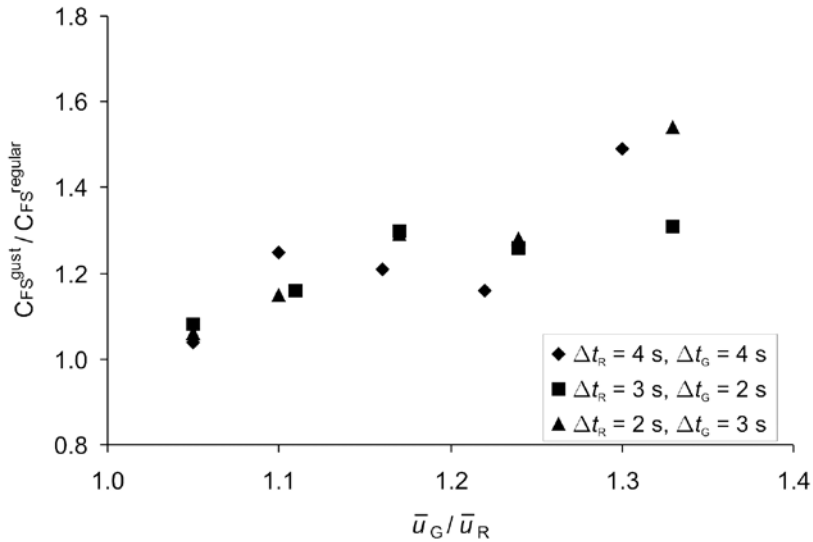


Figure 10. Mean side force experienced by a vehicle for various wind gust strengths and frequencies, Kozmar et al. (2012a)

Slika 10. Prosječna bočna sila vozila za različite jačine i frekvencije udara vjetrova, Kozmar i sur. (2012a)

The mean side force ($C_{FS}^{gust} / C_{FS}^{regular}$ ratio) increases linearly with an increase in the gust strength (\bar{u}_G / \bar{u}_R), where both C_{FS}^{gust} and $C_{FS}^{regular}$ were normalized using the same mean flow velocity \bar{u}_R . The average increase in the mean side force is about 16% larger than the increase in the mean flow velocity for all repetition rates. For the same \bar{u}_G / \bar{u}_R ratio, $C_{FS}^{gust} / C_{FS}^{regular}$ is within the $\pm 12\%$ margin.

Figure 11 shows an increase in the mean overturning moment around the vehicle center with an increase in the mean flow velocity.

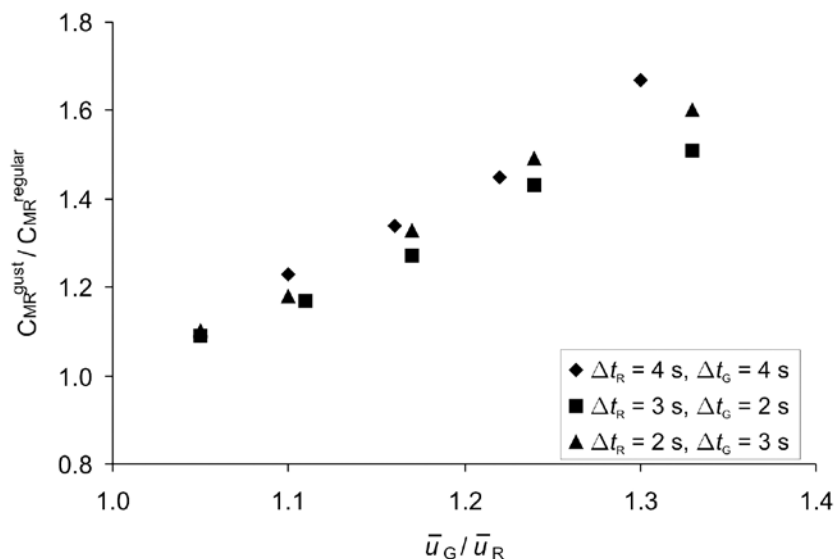


Figure 11. Mean overturning moment experienced by a vehicle for various wind gust strengths and frequencies, Kozmar et al. (2012a)

Slika 11. Prosječni moment prevrtanja vozila za različite jačine i učestalosti udara vjeta, Kozmar i sur. (2012a)

C_{MR}^{gust} is the mean overturning moment in wind gusts, and $C_{MR}^{regular}$ is the mean overturning moment in ‘regular’ wind. M_R was calculated by integrating the moments over the respective model surface around the center of gravity height using the pressure results over the vertical surfaces of the vehicle and its roof.

The mean overturning moment increases twice as strongly as the mean flow velocity, i.e. for a 10% increase in velocity, the overturning moment increases by 20%. For the same \bar{u}_G / \bar{u}_R ratio, the recorded $C_{MR}^{gust} / C_{MR}^{regular}$ is within the $\pm 10\%$ margin.

The frequency of wind gusts does not have a considerable effect on the mean side force and mean overturning moment as the results indicate the same trends in all these configurations.

Unsteady aerodynamic loads are particularly relevant for the dynamic stability of vehicles. In order to investigate this complex phenomenon, the side force and overturning moment fluctuations of the vehicle were analyzed, Figures 12-17. $S_{FS}(f)$ is the power spectral density of the side force fluctuations, and σ_{FS}^2 is their variance. $S_{MR}(f)$ is the power spectral density and σ_{MR}^2 is the variance of the overturning moment fluctuations.

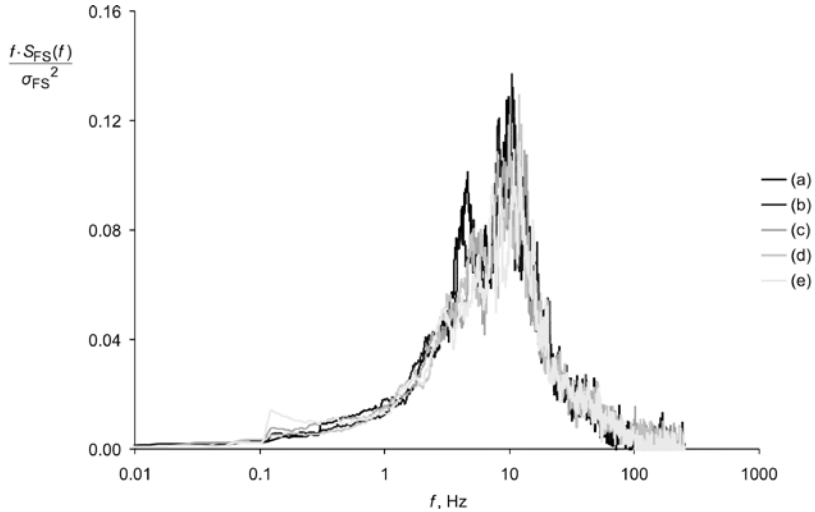


Figure 12. Power spectral density of the side force fluctuations for the time series presented in Table 1 ($\Delta t_R = 4$ s and $\Delta t_G = 4$ s), Kozmar et al. (2012a)

Slika 12. Spektralna gustoća snage pulzacija bočne sile za eksperimente navedene u Tablici 1 ($\Delta t_R = 4$ s and $\Delta t_G = 4$ s), Kozmar i sur. (2012a)

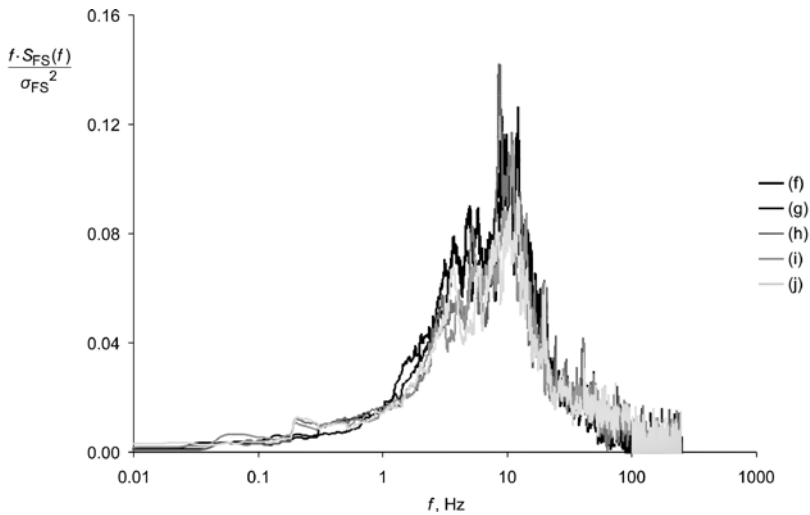


Figure 13. Power spectral density of the side force fluctuations for the time series presented in Table 2 ($\Delta t_R = 3$ s and $\Delta t_G = 2$ s), Kozmar et al. (2012a)

Slika 13. Spektralna gustoća snage pulzacija bočne sile za eksperimente navedene u Tablici 2 ($\Delta t_R = 3$ s and $\Delta t_G = 2$ s), Kozmar i sur. (2012a)

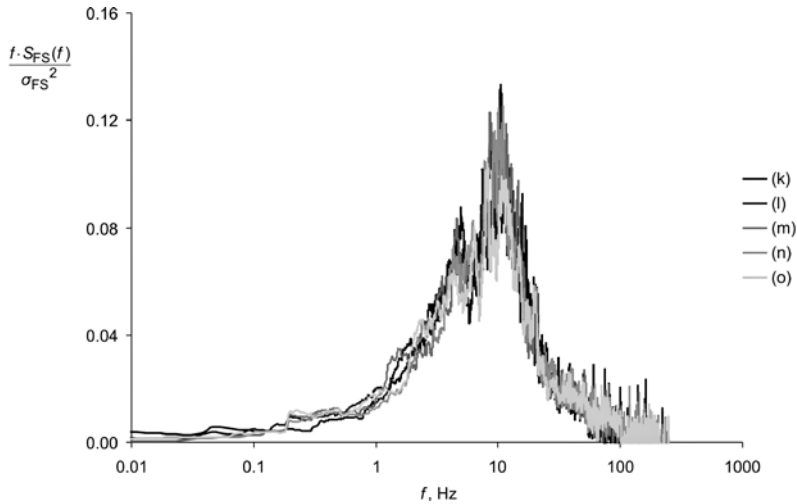


Figure 14. Power spectral density of the side force fluctuations for the time series presented in Table 3 ($\Delta t_R = 2$ s and $\Delta t_G = 3$ s), Kozmar et al. (2012a)

Slika 14. Spektralna gustoća snage pulzacija bočne sile za eksperimente navedene u Tablici 3 ($\Delta t_R = 2$ s and $\Delta t_G = 3$ s), Kozmar i sur. (2012a)

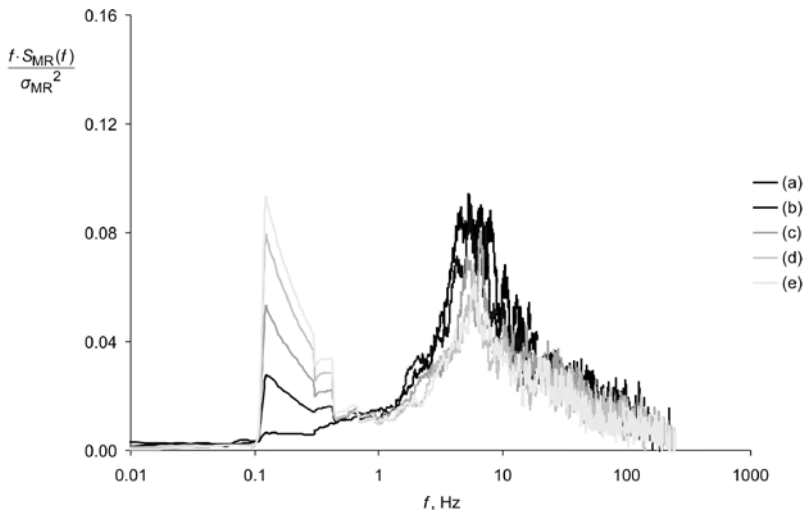


Figure 15. Power spectral density of the overturning moment fluctuations for the time series presented in Table 1 ($\Delta t_R = 4$ s and $\Delta t_G = 4$ s), Kozmar et al. (2012a)

Slika 15. Spektralna gustoća snage pulzacija momenta prevrtanja za eksperimente navedene u Tablici 1 ($\Delta t_R = 4$ s and $\Delta t_G = 4$ s), Kozmar i sur. (2012a)

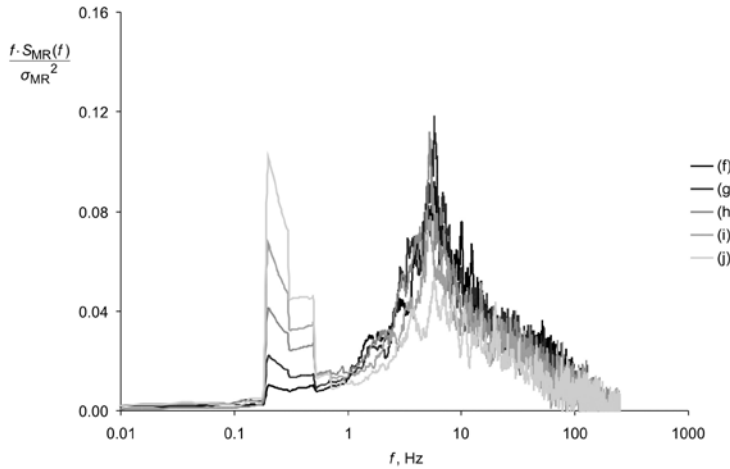


Figure 16. Power spectral density of the overturning moment fluctuations for the time series presented in Table 2 ($\Delta t_R = 3$ s and $\Delta t_C = 2$ s), Kozmar et al. (2012a)

Slika 16. Spektralna gustoća snage pulzacija momenta prevrtanja za eksperimente navedene u Tablici 2 ($\Delta t_R = 3$ s and $\Delta t_C = 2$ s), Kozmar i sur. (2012a)

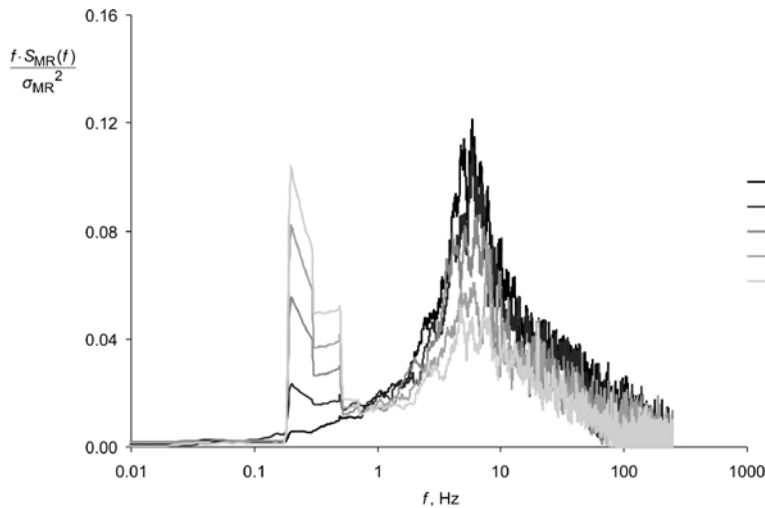


Figure 17. Power spectral density of the overturning moment fluctuations for the time series presented in Table 3 ($\Delta t_R = 2$ s and $\Delta t_C = 3$ s), Kozmar et al. (2012a)

Slika 17. Spektralna gustoća snage pulzacija momenta prevrtanja za eksperimente navedene u Tablici 3 ($\Delta t_R = 2$ s and $\Delta t_C = 3$ s), Kozmar i sur. (2012a)

For the F_s fluctuations, a distinct peak at 10 Hz due to buffeting vortices shed from the bridge deck is present in all configurations. The gust strength and frequency have negligible effects on the peak frequency and magnitude. The Strouhal number $St = fD/\bar{u} \sim 0.075$ was calculated using the peak frequency $f = 10$ Hz, $D \sim 0.03$ m (bridge-deck height including the barrier) and $\bar{u} = 4$ m/s, which is close to $St = 0.1$, a value which has commonly been accepted for the flow separation from bridge decks, Ryall et al. (2000).

Three spectral peaks are observed in the M_R fluctuations. These are low-frequency peaks at 0.125 Hz and 0.2 Hz (0.0125 Hz and 0.02 Hz full-scale) and the high-frequency peak at ~ 10 Hz (~ 1 Hz full-scale).

The low-frequency peak corresponds to the peak in the freestream wind spectrum. The high-frequency peak is a consequence of the vortex shedding from the bridge and the vehicle. This high-frequency peak is also observed in the F_s spectra. These results indicate that the M_R is concurrently affected by the vortex shedding and wind gusting phenomena. The low-frequency peak becomes stronger and the high-frequency peak weaker as the wind-gust strength increases. At the same time, the energy excited by the vortex shedding phenomenon decreases.

Another segment of work addressed the effect of α and the vehicle position on the bridge deck on the aerodynamic loads acting on the vehicle. In these experiments, the effects of Bora wind gusts were simulated by subjecting the vehicle and bridge-deck section models to an airflow which consisted of intermittent switching between ‘regular’ wind and wind gusts each 3 s. A portion of this velocity time record is shown in Figure 18.

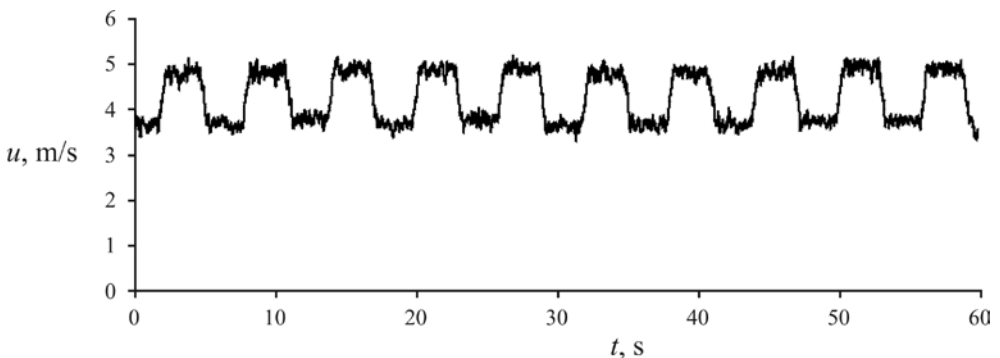


Figure 18. A portion of the studied velocity time record, Kozmar et al. (2015)

Slika 18. Dio vremenskog zapisa brzine, Kozmar i sur. (2015)

Steady aerodynamic loads, i.e. F_S and M_R , of the vehicle in the upwind and middle traffic lanes of the bridge deck subjected to Bora gusting were analyzed at various α , Figures 19 and 20. F_S and M_R were normalized using their respective values at $\alpha = 10^\circ$.

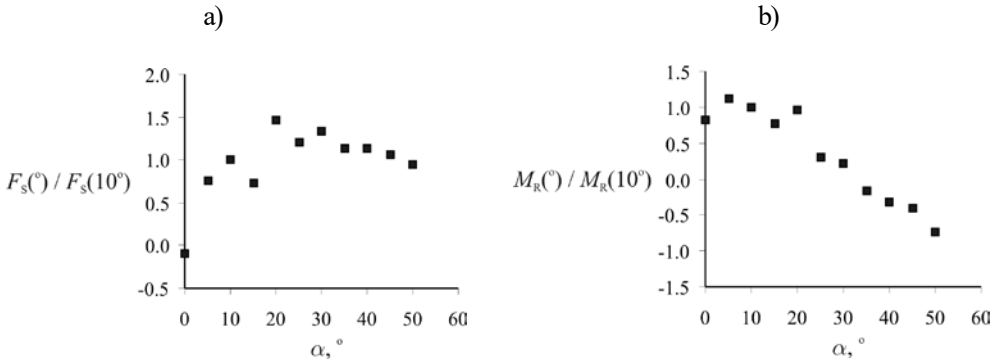


Figure 19. F_S and M_R of the vehicle in the upwind traffic lane at $\alpha = 0^\circ, 5^\circ, 10^\circ, 15^\circ, 20^\circ, 25^\circ, 30^\circ, 35^\circ, 40^\circ, 45^\circ, 50^\circ$; the horizontal flow incidence angle is 0° , Kozmar et al. (2015)

Slika 19. F_S i M_R vozila u prometnoj traci uz vjetar pri $\alpha = 0^\circ, 5^\circ, 10^\circ, 15^\circ, 20^\circ, 25^\circ, 30^\circ, 35^\circ, 40^\circ, 45^\circ, 50^\circ$; horizontalni kut nastrujavanja zraka je 0° , Kozmar i sur. (2015)

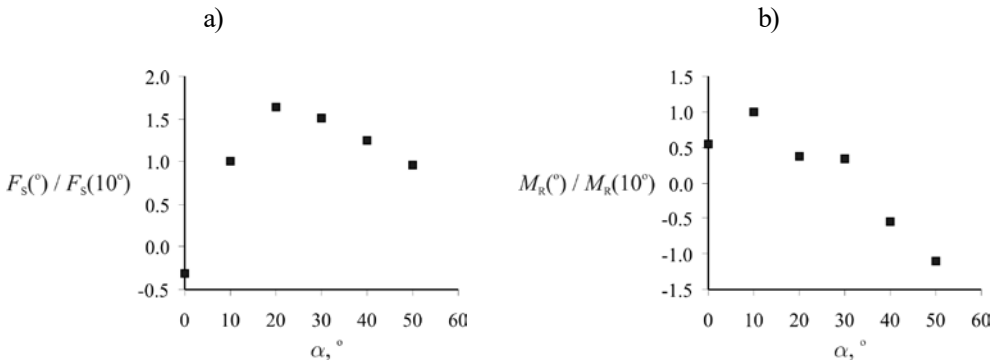


Figure 20. F_S and M_R of the vehicle in the middle traffic lane at $\alpha = 0^\circ, 10^\circ, 20^\circ, 30^\circ, 40^\circ, 50^\circ$; the horizontal flow incidence angle is 0° , Kozmar et al. (2015)

Slika 20. F_S i M_R vozila u srednjoj prometnoj traci pri $\alpha = 0^\circ, 10^\circ, 20^\circ, 30^\circ, 40^\circ, 50^\circ$; horizontalni kut nastrujavanja zraka je 0° , Kozmar i sur. (2015)

The trends observed for a vehicle in the upwind and middle traffic lanes are similar. F_s is minimal at $\alpha = 0^\circ$ because the barrier wall at the upwind leading edge of the bridge-deck section shelters the vehicle. With an increasing α , the vehicle becomes more exposed to the flow and the F_s reaches its maximum at $\alpha \sim 20^\circ$. With a further rise in α , the F_s decreases.

Small wind incidence angles around $\alpha = 10^\circ$ are critical in the context of the M_R , a trend which is present for both vehicle positions on the bridge deck. With a further gain in α , the M_R decreases. This trend at small α is due to: a) slight negative pressures on the upwind vehicle surface close to the ground due to the flow separating from the barrier wall and a consequent flow recirculation between the barrier wall and the upwind vehicle surface; or b) negative pressures on the vehicle top surface due to the flow separation. The higher risk for vehicles in these configurations is at $\alpha < 30^\circ$.

In order to analyze the unsteady aerodynamic loading of vehicles on bridges subjected to the Bora wind, S_{FS} , S_{MR} and the respective fluctuating (rms) aerodynamic coefficients $C_{FS,rms}$ and $C_{MR,rms}$ were studied.

Figures 21, 22, 23 show S_u in the freestream flow, and S_{FS} and S_{MR} along with their respective $C_{FS,rms}$ and $C_{MR,rms}$, respectively, all for the vehicle in the upwind traffic lane.

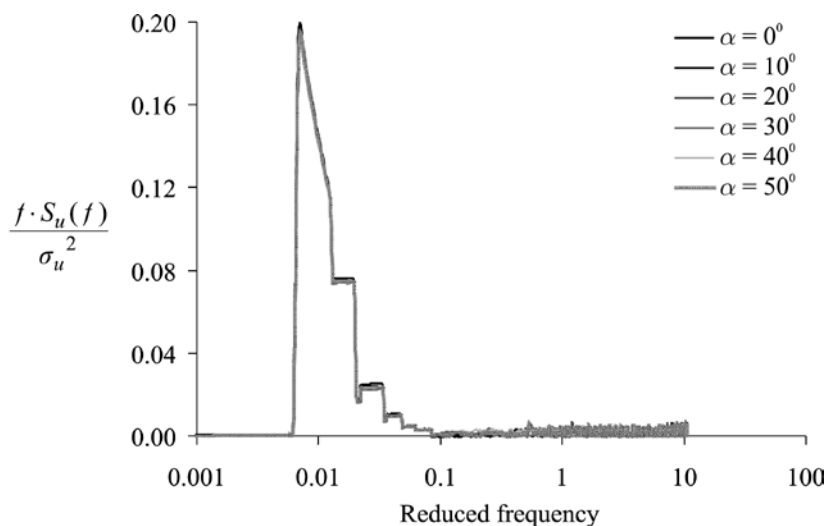
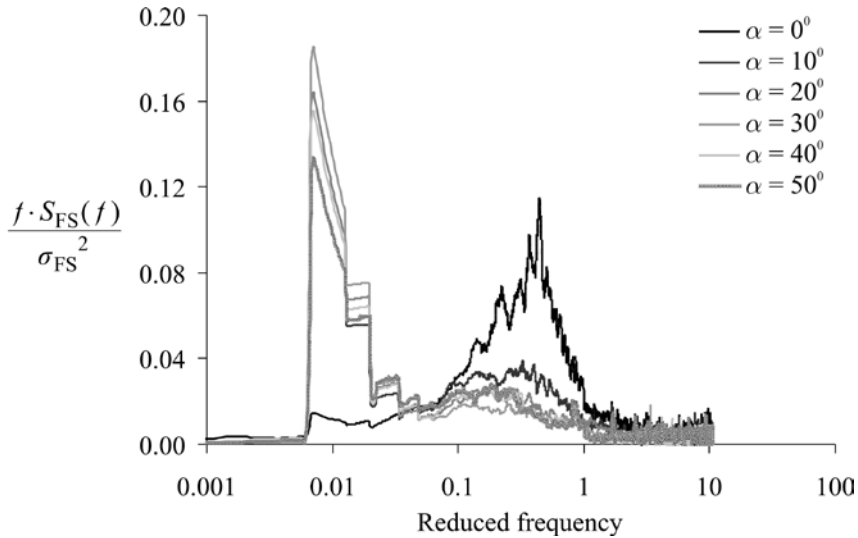


Figure 21. Power spectral density of the longitudinal flow velocity fluctuations, Kozmar et al. (2015)

Slika 21. Spektralna gustoća snage uzdužnih pulzacija brzine strujanja zraka, Kozmar i sur. (2015)



$\alpha, ^\circ$	0	10	20	30	40	50
$C_{FS,rms}, -$	0.37	0.47	0.49	0.54	0.44	0.38

Figure 22. Power spectral density and $C_{FS,rms}$ of the side force fluctuations, Kozmar et al. (2015)

Slika 22. Spektralna gustoća snage i $C_{FS,rms}$ pulzacija bočne sile, Kozmar i sur. (2015)

$\alpha, ^\circ$	0	10	20	30	40	50
$C_{MR,rms}, -$	0.22	0.22	0.19	0.16	0.14	0.15

Figure 23. Power spectral density and $C_{MR,rms}$ of the overturning moment fluctuations, Kozmar et al. (2015)

Slika 23. Spektralna gustoća snage i $C_{MR,rms}$ pulzacija momenta prevrtanja, Kozmar i sur. (2015)

In the velocity power spectra, there is a low-frequency peak which is a consequence of intermittent switching between lower and higher flow velocity. In the power spectra of the unsteady aerodynamic loads experienced by the vehicle, two peaks can be observed. The low-frequency peak at the same frequency as the characteristic frequency of the freestream wind gusting is due to the impact of the wind gusts. The high-frequency peak is attributed to the vortices shed from the bridge and their interactions with the vehicle model.

With an increasing α , the effects of shed vortices decrease, as exhibited by a weaker high-frequency peak in the power spectra of the unsteady aerodynamic loads experienced by the vehicle. $C_{FS,rms}$ reaches a maximum at $\alpha = 30^\circ$, while $C_{MR,rms}$ is maximal at $\alpha = 0^\circ$.

Another important aspect of the Bora cross-wind gusting of vehicles is the position of the vehicle on the bridge deck. To analyze this issue, steady aerodynamic loads for a vehicle placed in the upwind, middle, and downwind traffic lanes at vertical and horizontal wind incidence angles of 0° are shown in Figure 24. The F_S and M_R are normalized using their respective results recorded for the vehicle in the upwind traffic lane.

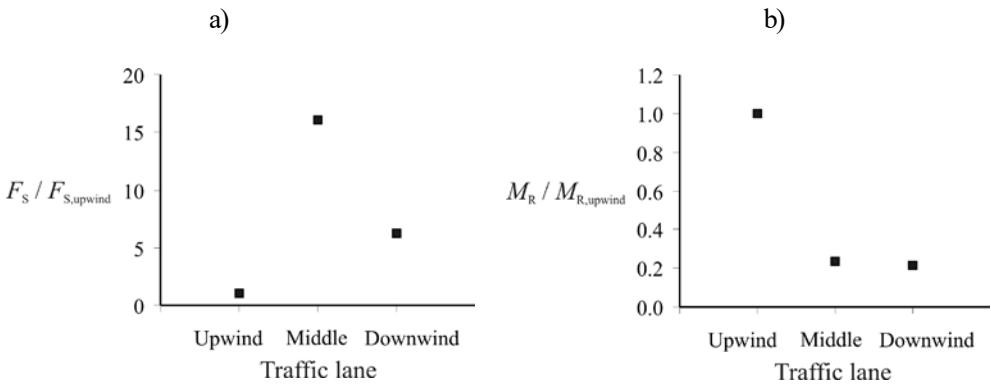


Figure 24. F_S and M_R of the vehicle in the upwind, middle, and downwind traffic lanes of the bridge-deck section, Kozmar et al. (2015)

Slika 24. F_S and M_R vozila u prometnim trakama uz vjetar, sredinu i niz vjetar na sekciji mosta, Kozmar i sur. (2015)

F_S is maximal in the middle traffic lane, while the M_R is maximal in the upwind traffic lane. These results indicate that in regard to steady aerodynamic loading, vehicles on bridges are more vulnerable when closer to the upwind edge of the bridge decks.

Figures 25, 26, 27 show S_u in the freestream flow, and S_{FS} and S_{MR} along with their respective $C_{FS,rms}$ and $C_{MR,rms}$ for a vehicle in the upwind, middle, and downwind traffic lanes, respectively, at horizontal and vertical flow incidence angles of 0° .

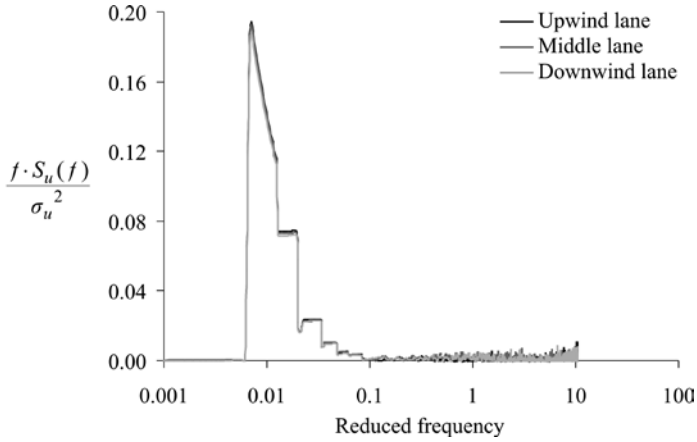
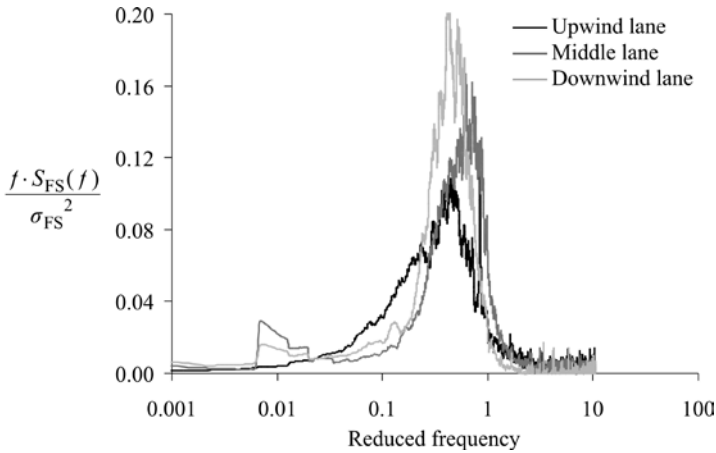


Figure 25. Power spectral density of longitudinal flow velocity fluctuations depending on the position of the vehicle on the bridge-deck section, Kozmar et al. (2015)

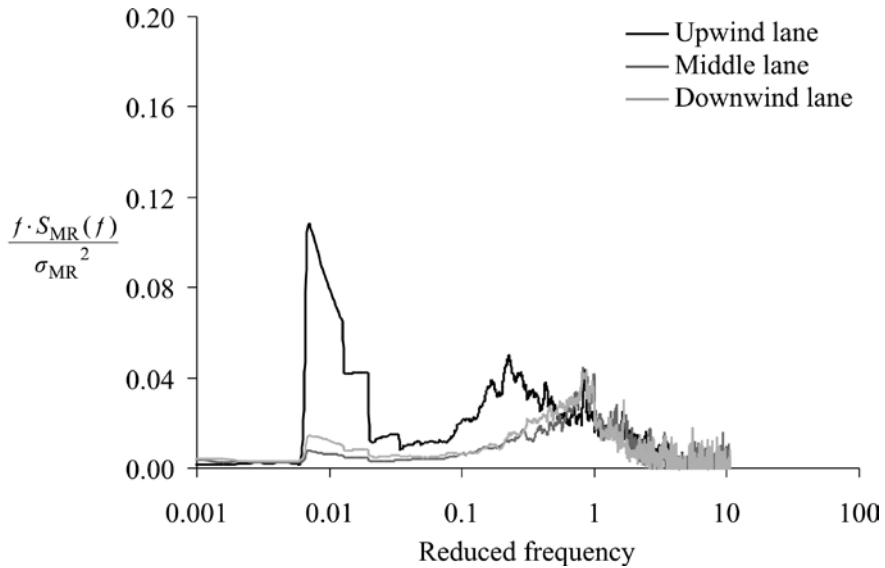
Slika 25. Spektralna gustoća snage uzdužnih pulzacija brzine strujanja zraka ovisno o položaju vozila na sekciji mosta, Kozmar i sur. (2015)



Traffic lane	Upwind	Middle	Downwind
$C_{FS,rms}$, -	0.31	0.45	0.42

Figure 26. Power spectral density and $C_{FS,rms}$ of the side force fluctuations depending on the vehicle position on the bridge-deck section, Kozmar et al. (2015)

Slika 26. Spektralna gustoća snage i $C_{FS,rms}$ pulzacija bočne sile ovisno o položaju vozila na sekciji mosta, Kozmar i sur. (2015)



Traffic lane	Upwind	Middle	Downwind
$C_{MR,rms}$ -	0.24	0.20	0.18

Figure 27. Power spectral density and $C_{MR,rms}$ of the overturning moment fluctuations depending on the vehicle position on the bridge-deck section, Kozmar et al. (2015)

Slika 27. Spektralna gustoća snage i $C_{MR,rms}$ pulzacija momenta prevrtanja ovisno o položaju vozila na sekciji mosta, Kozmar i sur. (2015)

As the vehicle is placed in the downstream traffic lanes, the high-frequency peak in the F_s fluctuations due to shed vortices becomes stronger. The low-frequency peak in the F_s fluctuations due to wind gusting is small for all three traffic lanes.

The low-frequency M_R fluctuations due to wind gusting are the strongest in the upwind traffic lane and negligible in the downwind traffic lanes. This indicates a weakening of the wind gusting effects on the M_R fluctuations when the vehicle is placed further downstream of the bridge-deck leading edge. The high-frequency M_R fluctuations due to shed vortices have nearly the same amplitude in all three traffic lanes, while they are slightly shifted to higher frequencies in the two downwind traffic lanes.

The $C_{FS,rms}$ coefficient is larger in the two downwind traffic lanes compared to the upwind traffic lane which is a consequence of an increase in the high-frequency peak due to shed vortices. This indicates a more dominant role of shed vortices in the F_s fluct-

tuations when the vehicle is placed further downstream of the bridge-deck leading edge. This is because of the reattachment of the flow that separated at the bridge-deck leading edge, a flow which subsequently hits the vehicle.

These unsteady aerodynamic loads reveal that the wind gusting frequency of local atmospheric winds can create difficulties in vehicle maneuvering and stability, particularly in the upwind traffic lane. The vulnerability of vehicles in the downwind traffic lanes is predominantly a consequence of shed vortices, which develop characteristics for a particular bridge architecture and the aerodynamic form of vehicles.

4. CONCLUSIONS

The Bora is a very strong and gusty downslope wind. It creates substantial aerodynamic loading and occasional dynamic instability of vehicles. Bora wind effects on road vehicles are currently not fully understood, which provided motivation for this work. In the present study, the experimental analysis of Bora wind loads on road vehicles is presented, and provides the authors' most relevant findings on this topic so far.

The experiments were carried out in the Transient Flow Field Simulator of the Nat-Haz Modeling Laboratory at the University of Notre Dame, USA. A vehicle model on the bridge-deck section model was subjected to an airflow which simulated Bora wind gusts. The analysis is based on the side force and overturning moment of the vehicle because these are the key parameters regarding aerodynamic loads acting on vehicles. These parameters were studied for various strengths and frequencies of Bora wind gusts, vertical wind incidence angles, and vehicle positions on the bridge deck.

In the experiments regarding the wind gust strength and frequency, the vehicle model was placed in the upwind traffic lane at zero horizontal and vertical flow incidence angles, where the flow perpendicularly impinged on the side surface of the vehicle model. The effect of the vertical wind incidence angle and vehicle position was analyzed for the vehicle model placed in the upwind, middle, and downwind traffic lanes of the bridge-deck section model. In these experiments, the horizontal flow incidence angle was zero, while the vertical flow incidence angle was studied from 0° to 50° . By varying the vertical flow incidence angle, these experiments aimed to simulate Bora wind loads on vehicles in the vicinity of hills characterized by various slope angles.

Regarding the wind gust strength and frequency experiments, the aerodynamic loads increase linearly with an increase in the gust strength. The average growth in the mean side force is $\sim 16\%$ higher than the increase in the mean flow velocity. The mean overturning moment increases twice as much as the mean flow velocity. The gust

strength and frequency have negligible effects on the peak frequency and magnitude. There is a peak in the side force spectra at frequencies corresponding to the energy contents exerted by the vortices shed from the bridge deck. In the overturning moment fluctuations, the low-frequency peak corresponds to the peak in the freestream wind spectrum, while the high-frequency peak is a consequence of the vortex shedding from the bridge deck and the vehicle. These results indicate that the overturning moment of the vehicle is concurrently influenced by the vortex shedding and wind gusting phenomena.

In the context of Bora wind loads acting on vehicles at various vertical wind incidence angles and vehicle positions on the bridge deck, steady aerodynamic loads on the vehicle are generally higher for vehicles closer to the upwind edge of the bridge decks.

The effect of the shed vortices on the side force fluctuations is dominant in the downstream traffic lanes, while the overturning moment fluctuations are at a maximum in the upwind traffic lane. These unsteady aerodynamic loads reveal that Bora wind gusting can create difficulties in vehicle maneuvering and stability in the upwind traffic lane, while the risk for vehicles in the downwind traffic lanes is predominantly a consequence of shed vortices, which depend on the particular bridge architecture and the aerodynamic form of the vehicles.

5. ACKNOWLEDGEMENTS

The first author acknowledges the support of the Fulbright Foundation and the University of Zagreb, Croatia. Support for the second author was partially provided by the Global Center of Excellence, Tokyo Polytechnic University, funded by the Japanese Ministry of Education, Culture, Sports, Science and Technology (MEXT) in the framework of the project on load effects in transient flow conditions. Special thanks go to Mr. Brent Bach for manufacturing the experimental models.

6. REFERENCES

- Bajić A (1988). The strongest Bora event during ALPEX SOP, *Rasprave-Papers* 23, 1-12.
- Bajić A (1989). Severe Bora on the northern Adriatic. Part I: Statistical analysis, *Rasprave-Papers* 24, 1-9.
- Baker CJ (1986). A simplified analysis of various types of wind-induced road vehicle accidents, *Journal of Wind Engineering and Industrial Aerodynamics* 22(1), 69-85.

Baker CJ (1987). Measures to control vehicle movement at exposed sites during windy periods, *Journal of Wind Engineering and Industrial Aerodynamics* 25(2), 151-161.

Baker CJ (1991a). Ground vehicles in high cross winds. 2. Unsteady aerodynamic forces, *Journal of Fluids and Structures* 5(1), 91-111.

Baker CJ (1991b). Ground vehicles in high cross winds. 3. The interaction of aerodynamic forces and the vehicle system, *Journal of Fluids and Structures* 5(2), 221-241.

Baker CJ (1991c). Ground vehicles in high cross winds. 1. Steady aerodynamic forces, *Journal of Fluids and Structures* 5(1), 69-90.

Baker CJ, Robinson CG (1990). The assessment of wind tunnel testing techniques for ground vehicles in cross winds, *Journal of Wind Engineering and Industrial Aerodynamics* 33(1-2), 429-438.

Baker CJ, Reynolds S (1992). Wind-induced accidents of road vehicles, *Accident Analysis and Prevention* 24(6), 559-575.

Bearman PW, Mullarkey SP (1994). Aerodynamic Forces on Road Vehicles due to Steady Side Winds and Gusts, Vehicle Aerodynamics Conference, Loughborough, United Kingdom.

Belušić D, Klaić, ZB (2004). Estimation of Bora wind gusts using a limited area model, *Tellus A: Dynamic Meteorology and Oceanography* 56(4), 296-307.

Belušić D, Klaić ZB (2006). Mesoscale dynamics, structure and predictability of a severe Adriatic Bora case, *Meteorologische Zeitschrift* 15(2), 157-168.

Belušić D, Hrastinski M, Večenaj Ž, Grisogono B (2013). Wind regimes associated with a mountain gap at the northeastern Adriatic Coast, *Journal of Applied Meteorology and Climatology* 52(9), 2089-2105.

Coleman SA, Baker CJ (1994). An experimental study of the aerodynamic behavior of high sided lorries in cross winds, *Journal of Wind Engineering and Industrial Aerodynamics* 53(3), 401-429.

Enger L, Grisogono B (1998). The response of bora-type flow to sea surface temperature, *Quarterly Journal of the Royal Meteorological Society* 124(548), 1227-1244.

Grisogono B, Belušić D (2009). A review of recent advances in understanding the meso- and micro-scale properties of the severe Bora wind, *Tellus A* 61(1), 1-16.

Hangan H, Kareem A (2021). *The Oxford Handbook of Non-synoptic Wind Storms Hazards*, Oxford University Press, Oxford, United Kingdom.

Horvath K, Ivatek-Šahdan S, Ivančan-Picek B, Grubišić V (2009). Evolution and Structure of Two Severe Cyclonic Bora Events: Contrast between the Northern and Southern Adriatic, *Weather and Forecasting* 24(4), 946-964.

Jeromel M, Malačić V, Rakovec J (2009). Weibull distribution of bora and sirocco winds in the northern Adriatic Sea, *Geofizika* 26(1), 85-100.

Jurčec V (1981). On mesoscale characteristics of Bora conditions in Yugoslavia, *Pure and Applied Geophysics* 119, 640-657.

Kozmar H, Butler K, Kareem A (2009). Aerodynamic loads on a vehicle exposed to cross-wind gusts: An experimental study, 7th Asia-Pacific Conference on Wind Engineering, Taipei, Taiwan.

Kozmar H, Butler K, Kareem A (2011). Effects of cross-wind gust strength on vehicle aerodynamics, 13th International Conference on Wind Engineering, Amsterdam, The Netherlands.

Kozmar H, Butler K, Kareem A (2012a). Transient cross-wind aerodynamic loads on a generic vehicle due to bora gusts, *Journal of Wind Engineering and Industrial Aerodynamics* 111, 73-84.

Kozmar H, Butler K, Kareem A (2012b). Aerodynamic loads on vehicles due to the gusty bora wind, 7th International Congress of Croatian Society of Mechanics, Zadar, Croatia.

Kozmar H, Butler K, Kareem A (2015). Downslope gusty wind loading of vehicles on bridges, *Journal of Bridge Engineering* 20(11), 04015008-1-04015008-11.

Kozmar H (2017). Characteristics of downslope windstorms for engineering applications [Special issue], *Wind and Structures* 24(6).

Lepri P, Kozmar H, Večenaj Ž, Grisogono B (2014). A summertime near-ground velocity profile of the Bora wind, *Wind and Structures* 19(5), 505-522.

Lepri P, Večenaj Ž, Kozmar H, Grisogono B (2015). Near-ground turbulence of the Bora wind in summertime, *Journal of Wind Engineering and Industrial Aerodynamics* 147, 345-357.

Lepri P, Večenaj Z, Kozmar H, Grisogono B (2017). Bora wind characteristics for engineering applications, *Wind and Structures* 24(6), 579-611.

Petkovšek Z (1987). Main Bora gusts - a model explanation, *Geofizika* 4, 41-50.

Poje D (1992). Wind persistence in Croatia, *International Journal of Climatology* 12(6), 569-586.

Ryall MJ, Parke GAR, Harding JE (2000). *The Manual of Bridge Engineering*, Thomas Telford, London, United Kingdom.

Ryan A, Dominy RG (1998). Aerodynamic forces induced on a passenger vehicle in response to a transient cross-wind gust at a relative incidence of 30°, *SAE Transactions 107(6): Journal of Passenger Cars*, 958-966.

Tutiš V (1988). Bora on the Adriatic Coast during ALPES SOP on 27 to 30 April 1982, *Rasprave-Papers* 23, 45-56.

Večenaj Ž, Belušić D, Grisogono B (2010). Characteristics of the near-surface turbulence during a bora event, *Annales Geophysicae* 28(1), 155-163.

Večenaj Ž, Belušić D, Grubišić V, Grisogono B (2012). Along-coast features of bora related turbulence, *Boundary-Layer Meteorology* 143, 527-545.

Vučetić V (1991). Statistical analysis of severe Adriatic Bora, *Croatian Meteorological Journal* 26, 41-51.

Yoshino MM (1976). *Local Wind Bora*, University of Tokyo Press, Tokyo, Japan.

EKSPERIMENTALNO MODELIRANJE UDARA BURE NA CESTOVNA VOZILA

Sažetak

Bura je vrlo jak i mahovit zavjetrinski vjetar koji puše iz smjera sjeveroistoka preko obalnih planinskih lanaca na istočnoj obali Jadranskog mora. Pripisuje se značajne poteškoće za inženjersku infrastrukturu, promet i život općenito. Dok su učinci kvazistacionarnog turbulentnog atmosferskog graničnog sloja na cestovna vozila trenutno prilično poznati, bura stvara nestacionarna aerodinamička opterećenja na vozila, koja još uvijek nisu u potpunosti shvaćena. Stoga su utjecaji udara bure na cestovna vozila eksperimentalno ispitani. Istraživanje je provedeno na modelu cestovnog vozila, što je prema našim saznanjima prva analiza ove vrste. Poseban je naglasak na aerodinamičnim silama i momentima vozila ovisno o jačini i učestalosti udara bure, kutu nastrojavanja vjetra i položaju vozila na mostu. U eksperimentima koji se odnose na jačinu i frekvenciju udara bure, model vozila je postavljen u prometnu traku neposredno uz naletni rub sekcije mosta, pri čemu su horizontalni i vertikalni kutovi nastrojavanja jednaki nuli. Utjecaj vertikalnog kuta nastrojavanja i položaja vozila je analiziran za model vozila postavljen uz vjetar, niz vjetar i u srednjoj prometnoj traci. Pritom je horizontalni kut nastrojavanja jednak nuli, dok je utjecaj vertikalnog kuta nastrojavanja proučavan od 0° do 50° . Eksperimenti su provedeni u simulatoru polja nestacionarnog strujanja zraka u sklopu NatHaz laboratorija Sveučilišta Notre Dame u SAD-u. Rezultati su otkrili neka važna saznanja. S obzirom na jačinu i frekvenciju udara bure, aerodinamička opterećenja se linearno povećavaju s povećanjem jačine udara bure i na njih istodobno utječu pojave odvajanja vrtloga od sekcije mosta i udara vjetra. Osrednjenjena aerodinamička opterećenja su općenito veća kod vozila smještenih bliže naletnom bridu sekcije mosta. Udari bure mogu stvoriti poteškoće kod upravljanja vozilom i njegovom stabilnosti u prometnom traku uz naletni brid sekcije mosta, dok je rizik za vozila u drugim prometnim trakama uglavnom posljedica odvajanja vrtloga od naletnog ruba sekcije mosta, što je karakteristično za aerodinamičke oblike mosta i vozila.

Ključne riječi: Mahoviti vjetar bura, aerodinamička opterećenja cestovnih vozila, laboratorijski eksperimenti.

Hrvoje Kozmar

Faculty of Mechanical Engineering and
Naval Architecture, University of Zagreb,
Ivana Lučića 5, 10000 Zagreb, Croatia

Ahsan Kareem

NatHaz Modeling Laboratory, University of
Notre Dame, IN 46556, Notre Dame, USA

Rad 549. Technical sciences 21(2022)

Nakladnik

HRVATSKA AKADEMIJA ZNANOSTI I UMJETNOSTI
Trg Nikole Šubića Zrinskog 11, 10000 Zagreb

Za nakladnika

Akademik Dario Vretenar, glavni tajnik

Grafička urednica i urednica na portalu Hrčak

Nina Ivanović

Digitalni identifikator objekta (DOI)

Kristina Polak Bobić

Naklada

200 primjeraka

Tisak

Stega tisak

Zagreb, veljača 2022.